Petroleum Science 23 (2026) 4985–4998

Contents lists available at ScienceDirect

Petroleum Science

journal homepage: www.keaipublishing.com/en/journals/petroleum-science

Original Paper

A novel in situ polymerizing gel–fiber composite system with enhanced strength and degradability for temporary plugging

Yu-Hui Yang [a], Jun-Cheng Su [a], Shan-Sheng Xu [a], Zhi-Yi Wei [b], Chu-Yu Kang [a], Zhuo-Zhuang Liu [a], Jie Geng [a], Hai Huang [c], Hai-Ming Fan [a,*]

[a] Shandong Key Laboratory of Oil and Gas Field Chemistry, School of Petroleum Engineering, China University of Petroleum (East China), Qingdao, 266580, Shandong, China
[b] Institute of Exploration and Development, Daqing Oilfield Company Ltd., Daqing, 163453, Heilongjiang, China
[c] School of Petroleum Engineering, Xi'an Shiyou University, Xi'an, 710065, Shaanxi, China

ARTICLE INFO

Article history:
Received 3 February 2026
Received in revised form
29 April 2026
Accepted 29 April 2026
Available online 4 May 2026

Edited by Yan-Hua Sun

Keywords:
Temporary plugging agent
Gel–fiber composites
High strength
Diverting fracturing stimulation

ABSTRACT

The plugging performance and degradation properties of temporary plugging agents remain critical challenges in diverting fracturing technology for deep, high-temperature reservoirs. Conventional particle–fiber systems are constrained by strict size-matching requirements and poor thermal stability, often failing to achieve reliable plugging in complex, high-temperature reservoirs. To overcome these limitations, this study presents a gel–fiber composite plugging strategy based on in situ gelation. This method employs a pre-gel solution as a carrier for fibers, with elevated temperatures inducing in situ polymerization to form a fiber-reinforced gel. Results demonstrate that the optimized pre-gel solution maintains low viscosity during surface preparation and wellbore flow, while rapidly gelling within 0.33 h at 180 °C, ensuring good injectability and controllable gelation. The incorporation of fibers significantly enhances the mechanical properties of the gel, increasing the elastic modulus from 180 Pa to over 3300 Pa and maintaining stability under cyclic shear strains ranging from 10% to 200%. In simulated fracture sealing experiments, the composite system achieved a sealing pressure gradient exceeding 49 MPa·m^{-1} for 2–3 mm fractures, representing a 2.8-fold increase compared to the pure gel system. Moreover, all components degrade into low-viscosity fluids under high-temperature conditions, facilitating flowback. This study provides a novel temporary plugging strategy for deep, high-temperature unconventional reservoirs, featuring high strength, degradability, and broad adaptability for efficient diverting fracturing.

1. Introduction

Unconventional oil and gas reservoirs typically exhibit unfavorable geological characteristics, including low porosity and low permeability, and generally require fracturing treatments for economic production (Chen et al., 2024; Li et al., 2022; Wang et al., 2025; Zhou et al., 2025). Temporary plugging and diverting fracturing (TPDF) is a promising reservoir stimulation technique, in which degradable plugging agents are injected into fractures to form temporary plugs, thereby diverting subsequent fracturing fluids into under-stimulated zones and enhancing the stimulated reservoir volume (Li et al., 2024; Wang et al., 2023a, 2023b). The effectiveness of TPDF largely depends on the temporary plugging agent's ability to provide both robust sealing performance and reliable degradability under complex downhole conditions while maintaining post-fracturing conductivity (Xu et al., 2023; Zhou et al., 2022).

A variety of temporary plugging agents have been developed, including temporary plugging balls, granular materials, fibers, gels, and their composite systems. Among these, particulate- and fiber-based agents are the most widely used (Feng et al., 2021; Huo et al., 2025; Li et al., 2025; Peng et al., 2025; Wang et al., 2024a; Yang et al., 2020; Zhang et al., 2022a, 2022b). Fiber-based plugging agents mainly function by forming a filter cake within the fracture. However, such structures tend to form prematurely at fracture constrictions and are prone to failure under increasing pressure

* Corresponding author.
E-mail address: haimingfan@126.com (H.-M. Fan).
Peer review under the responsibility of China University of Petroleum (Beijing).

https://doi.org/10.1016/j.petsci.2026.04.052

gradients. Furthermore, their plugging strength is relatively limited (Wang et al., 2023a, 2023c). Granular temporary plugging agents, on the other hand, rely on particle accumulation and bridging within fractures. The effectiveness of this mechanism is highly dependent on the match between particle size and fracture width; plugging is ineffective if particles are too small or too large (Zhao et al., 2025b; Zou et al., 2024b). To enhance plugging strength, researchers often combine fibers and particulates to form composite systems (Kibikas and Ingraham, 2025; Zou et al., 2024a, 2024c). In these systems, the fibrous network helps stabilize the accumulation and bridging of particles while filling the interstitial pores, contributing to a denser and more effective sealing structure (Yang et al., 2019, 2020). However, due to unknown subsurface fracture parameters and significant differences in properties such as size, shape, and density between particulates and fibers, achieving coordinated transport and stable plugging of these composite systems under downhole conditions remains highly challenging (Ren et al., 2024; Tian et al., 2024; Wang et al., 2024b; Zhao et al., 2025a). To address this, researchers have conducted extensive laboratory experiments to develop reliable design methodologies for composite formulations. For example, Xu et al. (2024) developed a quantitative model based on fracture width, material concentration, and size parameters, providing a foundational framework for optimizing composite blends. Nevertheless, due to the limitations of laboratory equipment simulations and the complexity of downhole geological conditions, existing methods still struggle to determine precise material ratios. This limits their ability to meet the reliability requirements for field operations (Li et al., 2023; Zhang et al., 2020).

To overcome the limitations of particulate–fiber systems in sealing strength and adaptability, the fiber–gel composite strategy has emerged as a promising alternative. For example, Chen et al. (2023) pre-encapsulated fibers within polyacrylamide gel balls. Upon injection, the outer gel degrades to release the fibers for plugging (Chen et al., 2023). This design behaves as a single particle phase during injection, facilitating fiber transport deeper into fractures, and achieves a sealing pressure gradient of 5.2 MPa·m^{-1} in a 2 mm fracture. Zhao et al. (2023) developed re-crosslinkable preformed gel particles (RPPGs) incorporating fibers. These particles can re-crosslink underground to form an integrated gel structure, with the fibers providing reinforcement. At a fiber content of 0.1%, the system achieved a plugging pressure gradient of approximately 1.2 MPa·m^{-1}. Research by Gussenov and Seright (2024) on gel–fiber composites for water shut-off applications demonstrated that, in narrow fractures, fiber-reinforced gel can impede brine flow up to 8.4 times more effectively than pure gel (Gussenov and Seright, 2024). The addition of fibers also enhances the gel's strength and viscosity under certain conditions. Cohen et al. (2010) developed a self-diverting acid system using fibers for carbonate reservoir acidizing. This system relies on fiber accumulation within the formation to create a temporary plug, diverting acid to enlarge the etched volume. Meanwhile, Li et al. (2018) designed a fiber suspension system to plug unconsolidated, high-permeability sand by leveraging interactions between fibers and sand grains to significantly improve formation strength and stability. Collectively, these studies demonstrate the considerable potential of combining fibers with gels to enhance the mechanical properties and structural integrity of materials. However, current research has predominantly focused on applications such as profile control, water shut-off, acidizing, and sand control. Therefore, developing a gel–fiber composite system for temporary plugging and diversion fracturing that combines high strength, broad adaptability, and reliable degradability remains a valuable direction for future research.

This study proposes a high-temperature degradable gel–fiber composite system based on in situ polymerization, designed to enhance both plugging strength and adaptability synergistically. The system utilizes a gel-forming fluid as a carrier, which can be easily injected into fractures due to its favorable flow properties. Once exposed to reservoir temperature, it polymerizes in situ to form a gel that acts as the primary plugging structure. Meanwhile, fibers dispersed within the system reinforce this structure, optimizing its mechanical performance. This strategy offers two key advantages. First, it eliminates the strict particle-size matching requirement inherent in particulate-based systems. Second, by carefully designing high-temperature initiators and crosslinkers, it allows precise control over both the gelling process and subsequent degradation behavior. This ensures not only the controlled formation of a high-strength sealing structure at reservoir temperature but also its subsequent degradation.

2. Materials and methods

2.1. Materials

Acrylamide (AM, industrial grade) was supplied by Baomo Biochemical Co., Ltd., Dongying, Shandong. 2-Acrylamido-2-methylpropanesulfonic acid (AMPS, 99%), triallylamine (TAA, 99%), and dicumyl peroxide (DCP, 98%) were all purchased from Macklin Reagent Co., Ltd. Sodium hydroxide (NaOH, AR) was provided by Sinopharm Chemical Reagent Co., Ltd. All chemicals were used as received without further purification.

The fibers (industrial grade) were supplied by an engineering materials manufacturer in Shandong. The main component of the fiber was polyacrylonitrile (PAN). The fibers had lengths ranging from 6 to 9 mm and an average diameter of approximately 10 μm. As shown in Fig. 1(a), the fibers were initially received in a bundled or agglomerated state. To enhance dispersion, a small-scale shear device was applied to break apart these fiber bundles prior to use. Fig. 1(b) shows the microscopic morphology of the fibers, with an average diameter of approximately 10 μm.

2.2. Preparation of gel–fiber composite temporary plugging agent

The preparation process of the gel–fiber composite temporary plugging agent is illustrated in Fig. 2. First, the fibers were dispersed using a small-scale shear device. AM and AMPS were then dissolved in deionized water and stirred for 15 min until complete dissolution. Next, the crosslinker TAA and initiator DCP were added to the solution and mixed thoroughly. The pH was then adjusted to 7.0±0.5 with a NaOH solution, yielding a homogeneous gel-forming fluid. The pre-dispersed fibers were added to the fluid and stirred to ensure uniform distribution, resulting in the final composite gel-forming fluid. The fluid was sealed in a glass vial and heated in an oven to form the gel–fiber composite plugging agent. For comparison, a pure gel sample was prepared by sealing and heating the gel-forming fluid without fibers. The fiber concentration was calculated according to Eq. (1):

$$w_{\text{fiber}} = \frac{m_{\text{fiber}}}{m_{\text{fiber}} + m_{\text{gel-forming fluid}}} \times 100\% \quad (1)$$

where w_{fiber} is the mass concentration of fibers; m_{fiber} is the mass of the fibers, g; $m_{\text{gel-forming fluid}}$ is the mass of the gel-forming fluid, g.

Gel strength was measured by the gel code method (Sydansk, 1988). Gelation time was defined as the duration required for the system to reach its maximum gel strength.

2.3. Viscoelastic properties

The rheological properties of the gel–fiber composite temporary plugging agent were measured using a rheometer (Anton

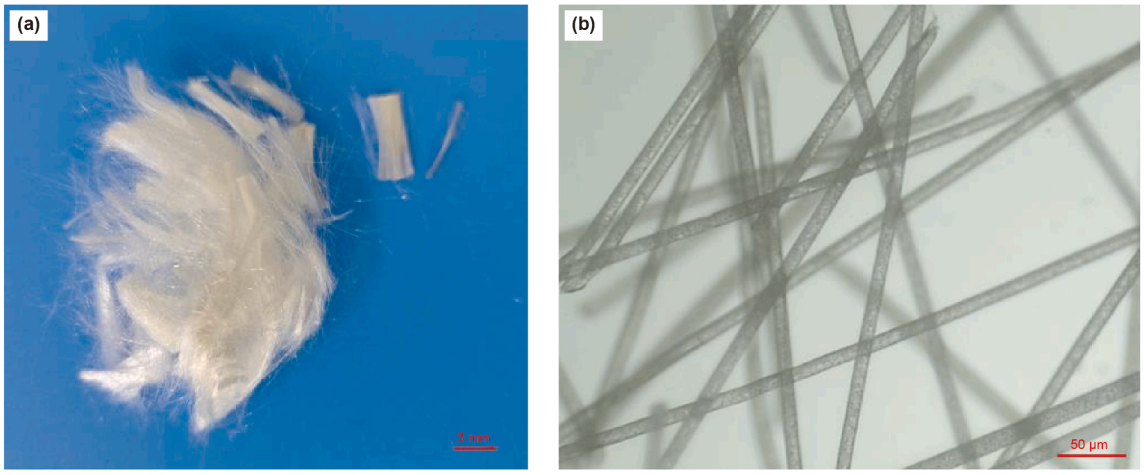

Fig. 1. Macroscopic (**a**) and microscopic (**b**) states of the fibers.

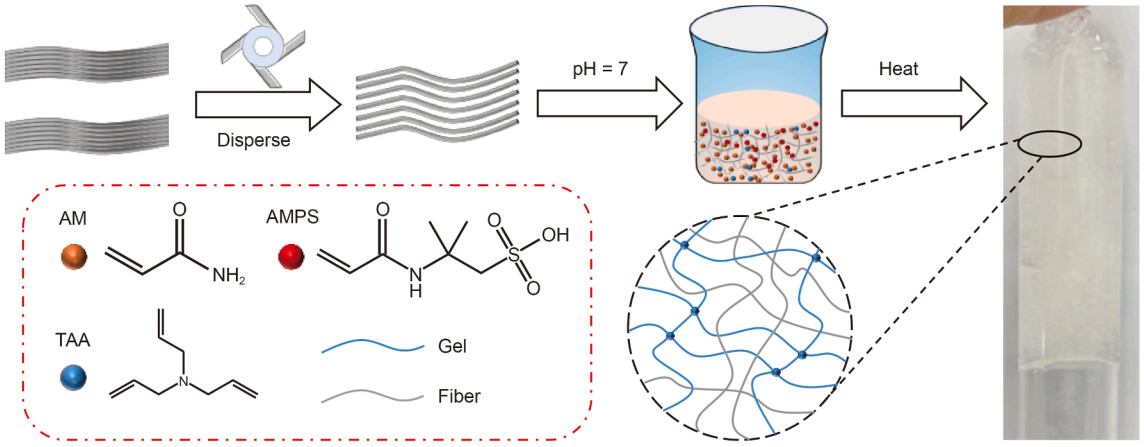

Fig. 2. Schematic diagram of the preparation process for gel–fiber composite temporary plugging agent.

Paar, MCR 302). In oscillatory mode, a parallel plate geometry (PP-50) with a 1 mm gap was used to measure the elastic modulus and structural stability at a fixed frequency of 1 Hz. The test sequence included seven consecutive cycles, each involving oscillation at 10% strain for 60 s followed by oscillation at 200% strain for 60 s. All oscillatory tests were conducted at 25 °C. The viscosity of the gel-forming fluid was measured in rotational mode at a constant shear rate of 7.34 s^{-1}. The shear-dependent viscosity of the degraded fluid was measured using a spindle (0#) over a shear rate range of 0.01 to 1000 s^{-1}. Both the viscosity measurements of the gel-forming fluid and the rheological tests of the degraded fluid were conducted at 80 °C.

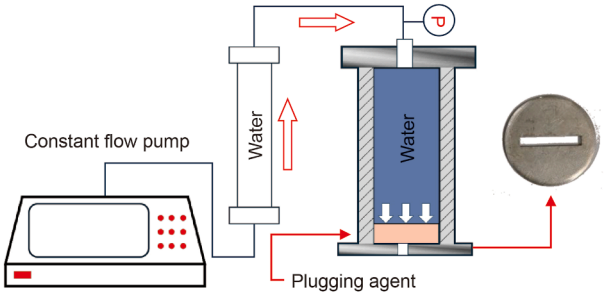

Fig. 3. Schematic of the test setup for pressure-bearing performance evaluation of the temporary plugging agent.

2.4. Plugging experiment at the fracture entrance

The pressure-bearing capacity of the composite temporary plugging agent at the fracture entrance was evaluated using the apparatus shown in Fig. 3. The apparatus consists of a syringe pump, an intermediate container, and a testing cell connected in series. The cylindrical testing cell has an inner diameter of 25 mm. A slotted stainless-steel spacer is placed at the bottom of the cell. For testing, a sample approximately 2 cm thick is first placed on the spacer, and the cell is then filled with water to transmit pressure. The syringe pump is activated to inject fluid at a constant rate of 1 mL·min^{-1}. Pressure variations are monitored in real time, and the outlet at the bottom of the cell is observed to detect any fluid breakthrough. The maximum recorded pressure is reported as the pressure-bearing capacity of the composite material.

2.5. Plugging experiment within the fracture

The fracture plugging performance was evaluated using the experimental setup shown in Fig. 4. To enable precise control of fracture width and ensure structural stability, a physical fracture model was prepared using a cement-casting method. The

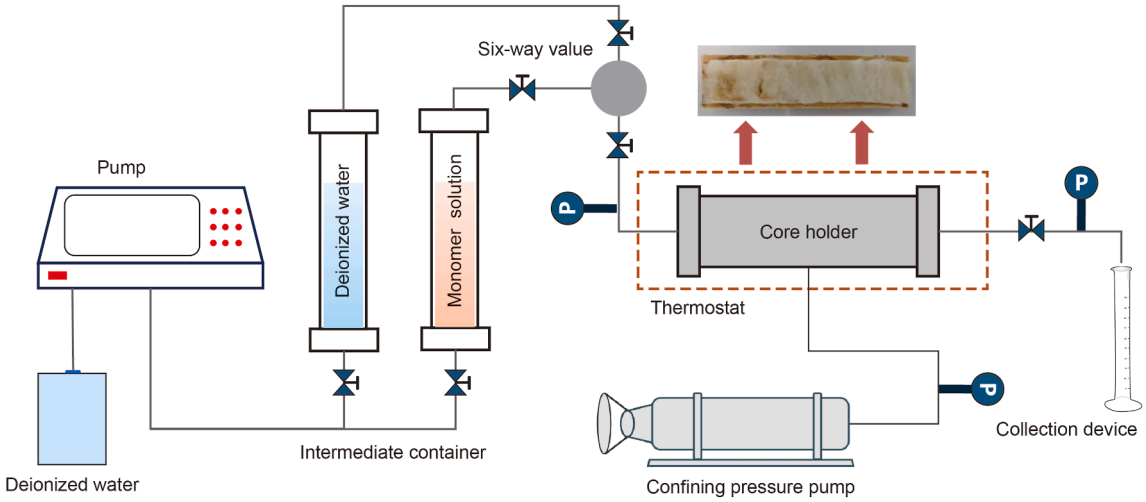

Fig. 4. Schematic of the test setup for evaluating core fracture plugging performance.

preparation procedure was as follows. First, cement mortar was poured into a high-density polyvinyl chloride (PVC) pipe with an outer diameter of 25 mm, a wall thickness of 2 mm, and a length of 10 cm. An acrylic plate (12 cm in length and 18 mm in width) was then inserted into the mortar-filled pipe. The assembly was cured in a cool, ventilated environment for 72 h. After curing, the acrylic plate was carefully removed, leaving a cement model with a simulated fracture. The fracture width was controlled by adjusting the thickness of the acrylic plate used during casting.

Prior to the injection of the gelling solution, fibers were pre-placed in the fracture space to simulate the presence of a fiber framework within the fracture. The fibers were carefully distributed along the fracture surface, and their distribution was adjusted to achieve a relatively uniform spatial arrangement. The fiber distribution within the fracture was verified using a split fracture model, as shown in Fig. 5. Due to the relatively low viscosity of the gel-forming fluid prior to gelation and the limited injection volume, disturbance to the pre-distributed fibers is considered minimal.

The outlet end of the fracture model was closed, and approximately one fracture volume (FV) of gel-forming fluid was injected. The inlet end was subsequently closed. The model was heated at 180 °C for 1 h to allow complete gelation. The outlet end of the core holder was opened, and a water flooding test was then conducted at 80 °C and a constant flow rate of 1 mL·min^{-1}, while the inlet pressure was continuously monitored. The maximum recorded pressure was used as the primary indicator of the sealing capacity of the composite temporary plugging agent.

2.6. Degradation evaluation of the gel and fibers

The extent of fiber degradation in aqueous solution was evaluated by measuring the residual solid mass after thermal aging using vacuum filtration. A fiber sample with a known initial mass (m_0) was accurately weighed and sealed in a glass ampule for high-temperature aging. After aging, the entire contents of the ampule were transferred and subjected to vacuum filtration through a membrane with a pore size of 2 μm. The undegraded solid residue retained on the membrane was dried and weighed to obtain the final mass (m_1). The fiber degradation rate was then calculated using Eq. (2):

$$R_{\text{degradation}} = \frac{m_0 - m_1}{m_0} \times 100\% \tag{2}$$

where $R_{\text{degradation}}$ is the degradation ratio.

In addition, based on our previous work (Yang et al., 2026), this study adopts the gel code method to evaluate the degradation of the gel phase. The gel phase degrades to a fully flowable state when its strength reaches Code A.

Fig. 5. Distribution of fibers within the fracture.

2.7. Structural characterization

The microscopic network structure of the gel was examined using a scanning electron microscope (Tescan MIRA 3). Samples of the composite temporary plugging agents were freeze-dried to maintain their internal structures. To enhance image quality, the freeze-dried samples were sputter-coated with a thin gold layer before imaging.

The molecular structure of the composite plugging agent was analyzed using a Fourier-transform infrared (FT-IR) spectrometer (Thermo Fisher Scientific, Nicolet 6700). Spectra were collected over a wavenumber range of 4000–400 cm^{-1} with a resolution of 4 cm^{-1}. The samples for FT-IR analysis were similarly prepared by freeze-drying.

3. Results and discussion

3.1. Injection fluidity and in situ gel formation performance

Gelation time is a critical parameter governing the injectability of the composite system. Ideally, the gelling fluid should maintain a low viscosity and flow readily during pumping, while rapidly polymerizing into a gel after entering fractures. Accordingly, a single-variable experimental approach was employed to systematically investigate the effects of monomer concentration, crosslinker concentration, initiator concentration, and temperature on gelation time. The corresponding results are presented in Fig. 6. The base formulation consisted of 8 wt% monomer, 0.12 wt% crosslinker, and 0.15 wt% initiator, with the mass ratio of AM to

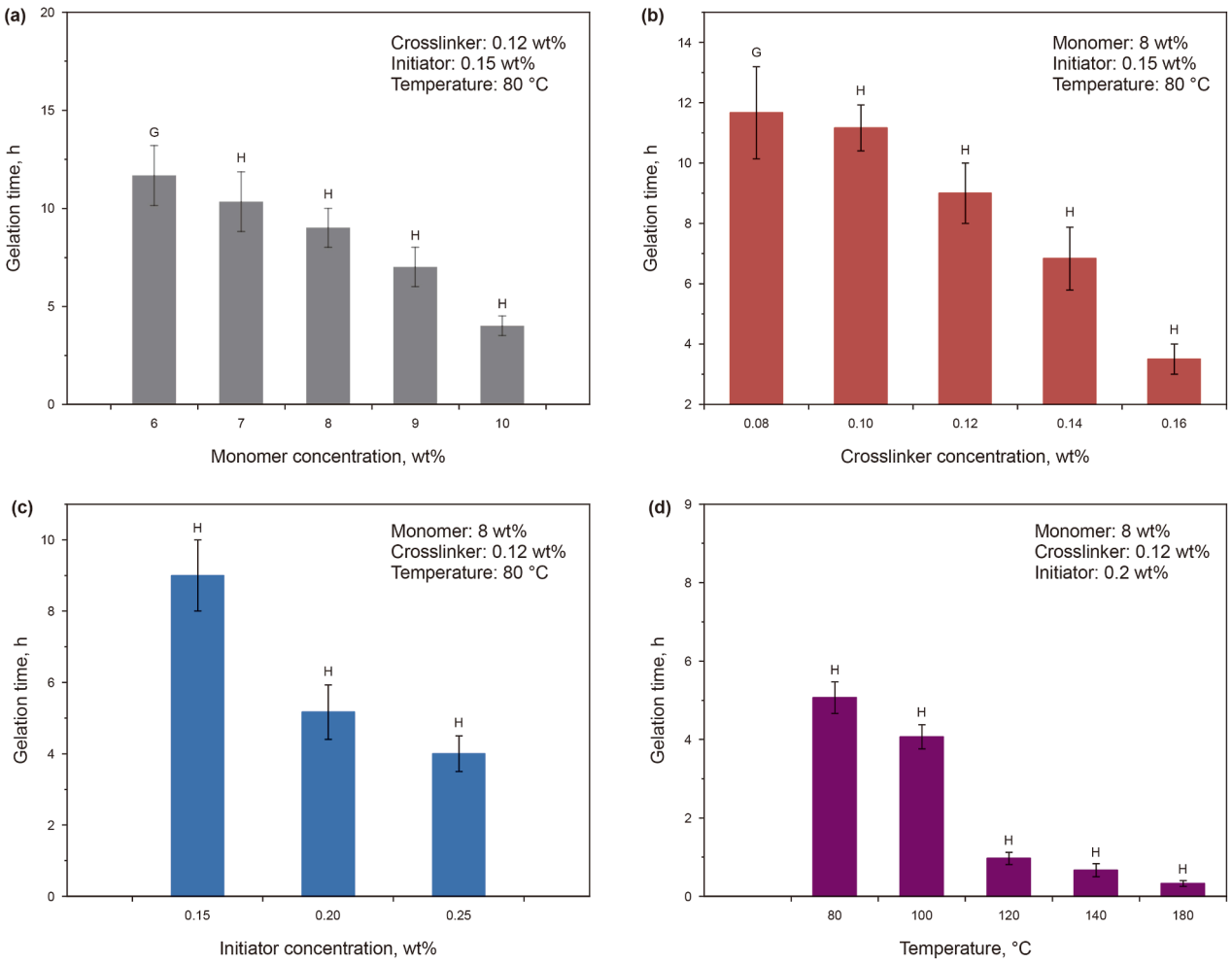

Fig. 6. Effects of monomer concentration (**a**), crosslinker concentration (**b**), initiator concentration (**c**), and temperature (**d**) on the gelation time of the gel matrix.

AMPS fixed at 4:1 based on previous work (Yang et al., 2026). In field operations, the temperature experienced by the fluid increases gradually during injection. Therefore, evaluating gelation time solely at the target reservoir temperature may overestimate the effective pumping window. To better simulate downhole thermal conditions during transport, 80 °C was selected as the evaluation temperature, corresponding to the mid-reservoir region. At this temperature, the influence of each formulation parameter on gelation time was examined. As shown in Fig. 6(a)–(c), increasing the concentrations of monomer, crosslinker, or initiator consistently shortened the gelation time. This behavior is attributed to higher reactant concentrations, which increase the number of active sites, accelerate the free-radical polymerization rate, and promote faster formation of the gel network. Notably, all tested formulations exhibited high gel strength, indicating that gelation time can be tuned over a wide range without compromising the structural integrity of the resulting gel. Considering both the field pumping time window and the requirement for rapid solidification within fractures, the optimized formulation was determined to be 8 wt% monomer, 0.12 wt% crosslinker, and 0.2 wt% initiator. The effect of temperature on gelation time is illustrated in Fig. 6(d). Gelation time decreased markedly with increasing temperature due to the enhanced free-radical generation rate and accelerated chain-growth reactions. At 180 °C, the system gelled within 0.33 h. Based on the geothermal gradient, a temperature of 180 °C corresponds to an estimated reservoir burial depth of approximately 6000–8000 m. However, during actual field operations, the injected fracturing fluid exerts a significant cooling effect on the wellbore and near-wellbore formation. For example, Li et al. (2024a) reported that when the fracturing fluid was injected at a rate of 4 $m^3 \cdot min^{-1}$ for 40 min, the formation temperature at a depth of 7000 m decreased to approximately 100 °C. These results demonstrate that the optimized gelling fluid exhibits good high-temperature adaptability, enabling long-distance pumping through the wellbore while rapidly forming an effective plugging gel upon reaching the target zone.

Fig. 7 presents the viscosity evolution of the gelling fluid during thermal aging at different temperatures. As shown in Fig. 7(a), at 25 and 50 °C, the viscosity remained low over 24 h with no noticeable increase, indicating good storage stability and the absence of premature polymerization in surface facilities and cooler wellbore sections. Fig. 7(b) further shows the time-dependent viscosity behavior in the temperature range of 80–180 °C. At 80 °C, the viscosity remained below 15.45 mPa·s during the initial aging stage ($\leq$ 250 min), followed by a sharp increase to 18,546 mPa·s at 300 min, indicating the onset of rapid gelation. At 100 °C, the low-viscosity state persisted for approximately 120 min. In contrast, at 140 and 180 °C, the viscosity increased rapidly with aging time, reflecting a significantly accelerated polymerization. Overall, these results confirm that the gelling fluid maintains low viscosity during preparation and

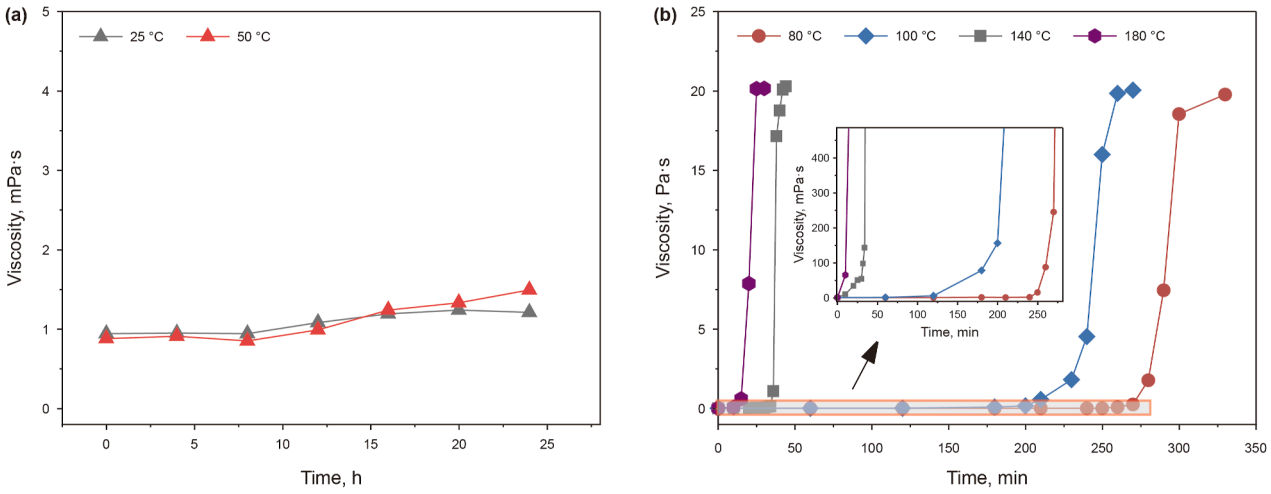

Fig. 7. Changes in the viscosity of the gelling fluid at different temperatures.

pumping, ensuring good injectability, while undergoing rapid viscosity buildup and gelation upon exposure to high reservoir temperatures.

Fig. 8 presents the dispersion and suspension stability of fibers in the gelling fluid under different concentrations and temperatures. Three fiber concentrations (0.6, 1.0, and 5.0 wt%) were assessed. The samples were kept at 25 and 50 °C for 24 h; at 140 and 180 °C, they were treated for 1 h. At all tested concentrations, the fibers exhibited favorable suspension stability in the gelling fluid, with no obvious sedimentation observed. At 140 and 180 °C, the gelling fluid polymerized into a gel within 1 h. After gelation, the fibers remained well suspended throughout the gel matrix. These results demonstrate good compatibility and stability between fibers and the gel system.

Fig. 9 further presents the gelation time and maximum gel strength of the composite temporary plugging agent at different fiber concentrations. The results indicate that increasing fiber concentration slightly shortens the gelation time of the composite, while the gel strength remains consistently Code H. The fibers do not participate in the primary cross-linking reaction between monomers and crosslinker in the gelling fluid. Therefore, the addition of fibers has a negligible effect on the gelling time of the fluid. This outcome provides a basis for further optimizing the mechanical reinforcement of the system by adjusting the fiber concentration.

Fig. 10 presents the elastic modulus and shear stability of the composite temporary plugging agent. As shown in Fig. 10(a), fiber concentrations below 1 wt% have no significant effect on the elastic modulus. At a fiber concentration of 3 wt% or higher, the elastic modulus increases by an order of magnitude compared to the pure gel and continues to rise with increasing fiber concentration. This increase is attributed to physical entanglement between fibers and polymer chains, which reinforces the network structure of the composite. As shown in Fig. 10(b) and (c), the elastic modulus of the composite system decreases significantly when the strain reaches 200%. Notably, the elastic modulus of the composite plugging agent demonstrates excellent stability throughout the testing process, regardless of fiber concentration. After seven loading–unloading cycles, the elastic modulus remains largely at its initial value. This indicates robust interfacial bonding and structural integrity within the composite system.

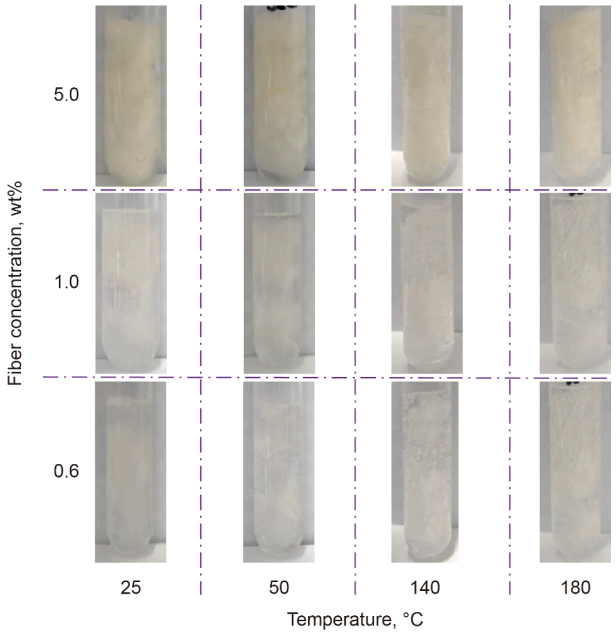

Fig. 8. Macroscopic dispersion states of fibers at different concentrations in gelling fluid under various temperatures.

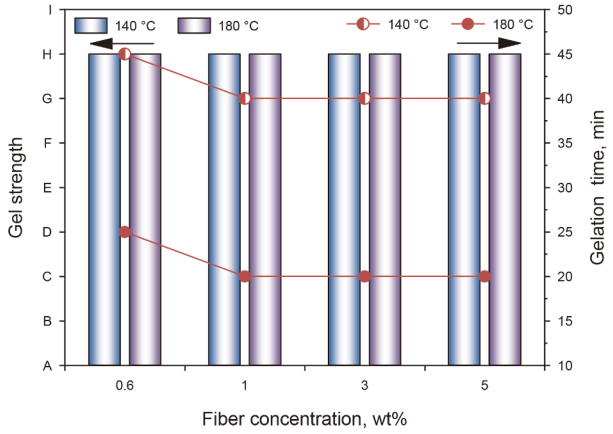

Fig. 9. Effect of fiber concentration on gel strength and gelation time of the composite system at different temperatures.

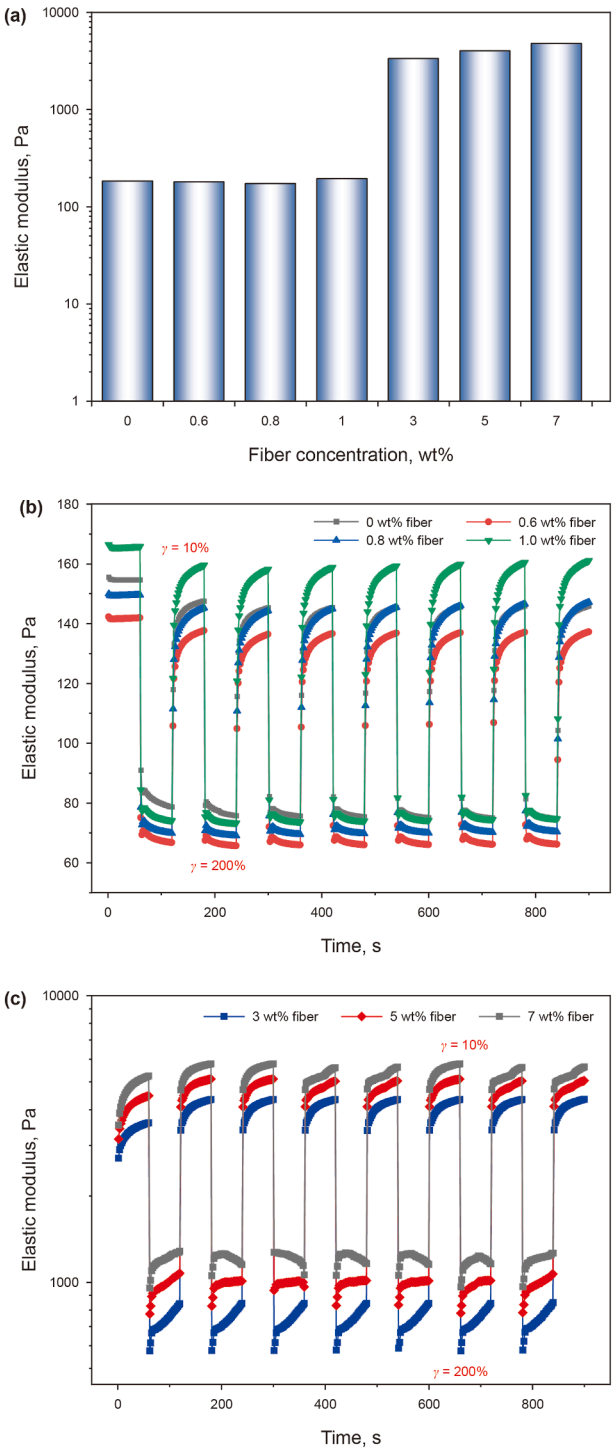

Fig. 10. (**a**) Effect of fiber concentration on the elastic modulus of the composite system; (**b**, **c**) cyclic shear performance tests.

3.2. Plugging performance of gel–fiber composite system

This study separately evaluated the sealing performance of the gel–fiber composite temporary plugging system at the fracture entrance and within the fracture interior. Fig. 11 illustrates the influence of fiber concentration, fracture width, and monomer concentration on the pressure-bearing capacity of the composite plugging agent at the fracture entrance. As shown in Fig. 11(a), the fiber concentration significantly affects the maximum pressure sustained by the composite. At a fiber concentration of 0 wt%, the pure gel withstands a maximum pressure of 180 kPa. Increasing the fiber concentration to 1 wt% does not noticeably improve pressure-bearing capacity. However, Fig. 11(b) reveals that the interwoven network formed by the fibers within the gel matrix enhances the system's spatial support. This network effectively delays the onset of a sharp pressure drop and impedes migration of the composite through the fracture. At fiber concentrations of 3–5 wt%, the network structure within the gel becomes denser, resulting in a marked improvement in pressure-bearing performance. At a fiber concentration of 7 wt%, the composite plugging agent attains a maximum pressure-bearing capacity of 2720 kPa.

With the fiber concentration fixed at 5 wt%, the effect of fracture width on the pressure-bearing performance of the composite plugging agent at the fracture entrance was further investigated, as shown in Fig. 11(c) and (d). As shown in Fig. 11(c), when the fracture width was reduced to 1 mm, the composite plugging agent formed a continuous and dense sealing layer, with its maximum pressure-bearing capacity increased to 3430 kPa. As the fracture width increased, the maximum pressure-bearing capacity of the composite decreased continuously. At a fracture width of 5 mm, the maximum pressure-bearing capacity was only 110 kPa. Furthermore, Fig. 11(d) indicates that as the fracture width increased, the pressure drop after reaching the maximum pressure-bearing capacity became more rapid. This behavior can be attributed to the difficulty of maintaining structural integrity of the plugging agent in wider fractures, where localized failure and rapid loss of sealing effectiveness are more likely to occur.

Fig. 11(e) and (f) illustrates the effect of monomer concentration on the pressure-bearing capacity of the composite plugging agent. As the monomer concentration increased, the crosslinking density and compactness of the gel network were significantly enhanced. This enhancement strengthens the mechanical integrity of the composite, resulting in a steady increase in its maximum pressure-bearing capacity. At a monomer concentration of 10 wt%, the maximum pressure-bearing capacity reached 1150 kPa. Conversely, when the gel network was weaker, the pressure dropped more rapidly after reaching its maximum. This indicates that a less robust gel network is more susceptible to sudden failure under applied pressure.

The sealing performance of the composite plugging agent within fractures is shown in Fig. 12. During the experiment, fibers were first placed inside the fracture at a concentration of 3 wt%, followed by injection of 1 fracture volume (FV) of gelling fluid. As shown in Fig. 12(a) and (b), during continuous injection of the subsequent fluid, the inlet pressure first increased and then decreased. The maximum pressure gradient decreased progressively with increasing fracture width: 53.47 MPa·m^{-1} at 2 mm, 49.9 MPa·m^{-1} at 3 mm, 22.55 MPa·m^{-1} at 4 mm, and 4.08 MPa·m^{-1} at 5 mm. Fig. 12(c) and (d) presents the plugging performance of the pure fiber system in fractures with different widths. When an equivalent amount of fiber was placed without gelling fluid injection, the inlet pressure gradually increased during water flooding and eventually stabilized. This behavior occurred because fibers became entangled under water flow, forming a permeable plugging structure. Once the pressure difference reached a critical value, a dynamic equilibrium was established, resulting in limited plugging capacity. The plugging performance of the pure gel system in fractures with different widths was further evaluated, as shown in Fig. 12(e) and (f). The inlet pressure increased initially but then dropped rapidly, indicating rapid structural failure of the gel after breakthrough. In contrast, the pressure decline in the composite system was more gradual, indicating that fiber

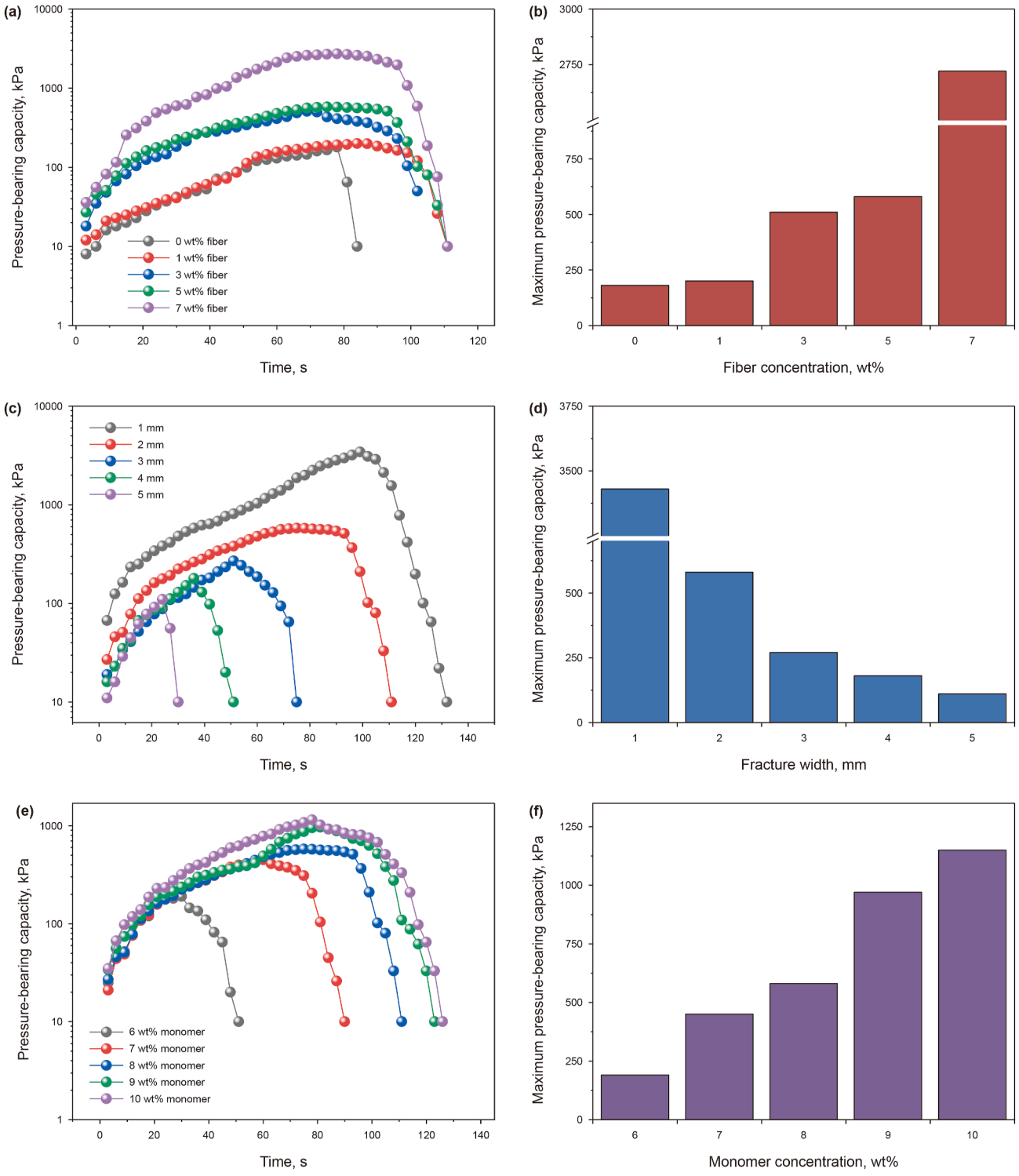

Fig. 11. Effects of fiber concentration (**a**, **b**), fracture width (**c**, **d**), and monomer concentration (**e**, **f**) on the pressure-bearing performance of the composite system.

incorporation enhanced overall structural strength and allowed partial sealing to be maintained after localized breakthrough. Quantitatively, the maximum pressure gradient of the pure gel in a 2 mm fracture ranged only from 19.18 to 14.9 MPa·m^{-1}. In summary, for fracture widths of 2 and 3 mm, fiber incorporation in the composite system enhanced plugging strength by approximately 2.8 and 3.4 times, respectively, compared with the pure gel system.

3.3. Degradation properties of gel–fiber composite system

Fig. 13 illustrates the thermal degradation behavior of the fibers in deionized water. As shown in Fig. 13(a), after 2 h of aging, the fiber structure remained intact, and no significant mass loss was detected by the membrane filtration test. With prolonged aging, the fibers gradually degraded, while the overall degradation ratio remained relatively low. Macroscopic observations in Fig. 13(b)

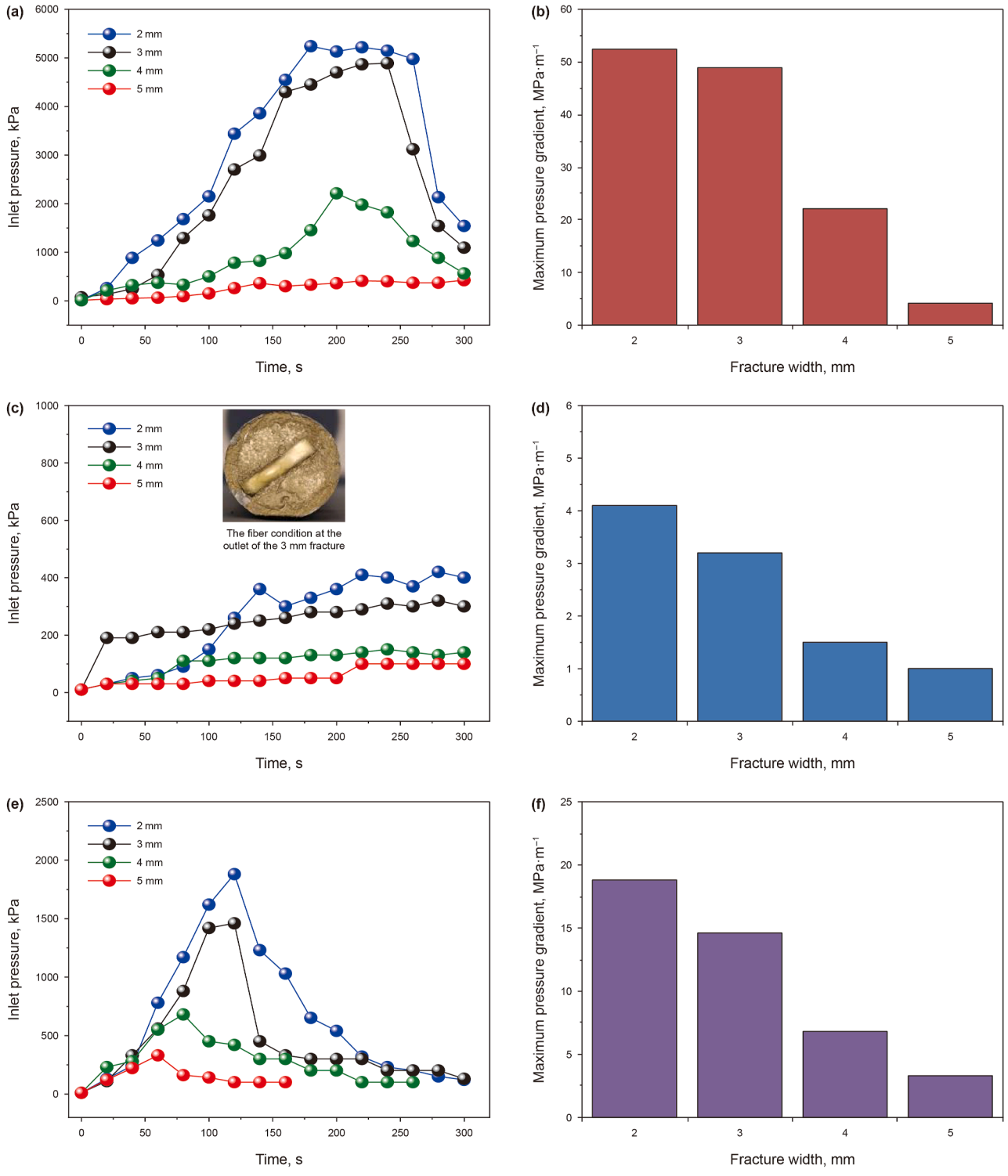

Fig. 12. Plugging performance of composite temporary plugging agent (**a**, **b**), pure fiber system (**c**, **d**), and pure gel system (**e**, **f**) in a fracture model.

show that most fibers remained visible to the naked eye prior to 15 h of aging. After 15 h, the solution in the ampoule turned brown, the fibers shortened noticeably, and the degraded solution became turbid. After 24 h of aging, the degraded solution further darkened and became transparent, indicating extensive fiber degradation.

Using a degradation ratio of 90% as the criterion for efficient fiber degradation, Fig. 14 shows the degradation time of the fibers in deionized water at different temperatures. The results indicate that at 140, 150, 160, 170, and 180 °C, the fibers required 10, 5, 2.5, 2, and 1 d, respectively, to reach efficient degradation. Higher temperatures significantly accelerated fiber degradation by enhancing molecular thermal motion and promoting chemical bond cleavage, which shortened the degradation cycle. These results demonstrate that the fibers used in this study exhibit efficient degradability under high-temperature conditions.

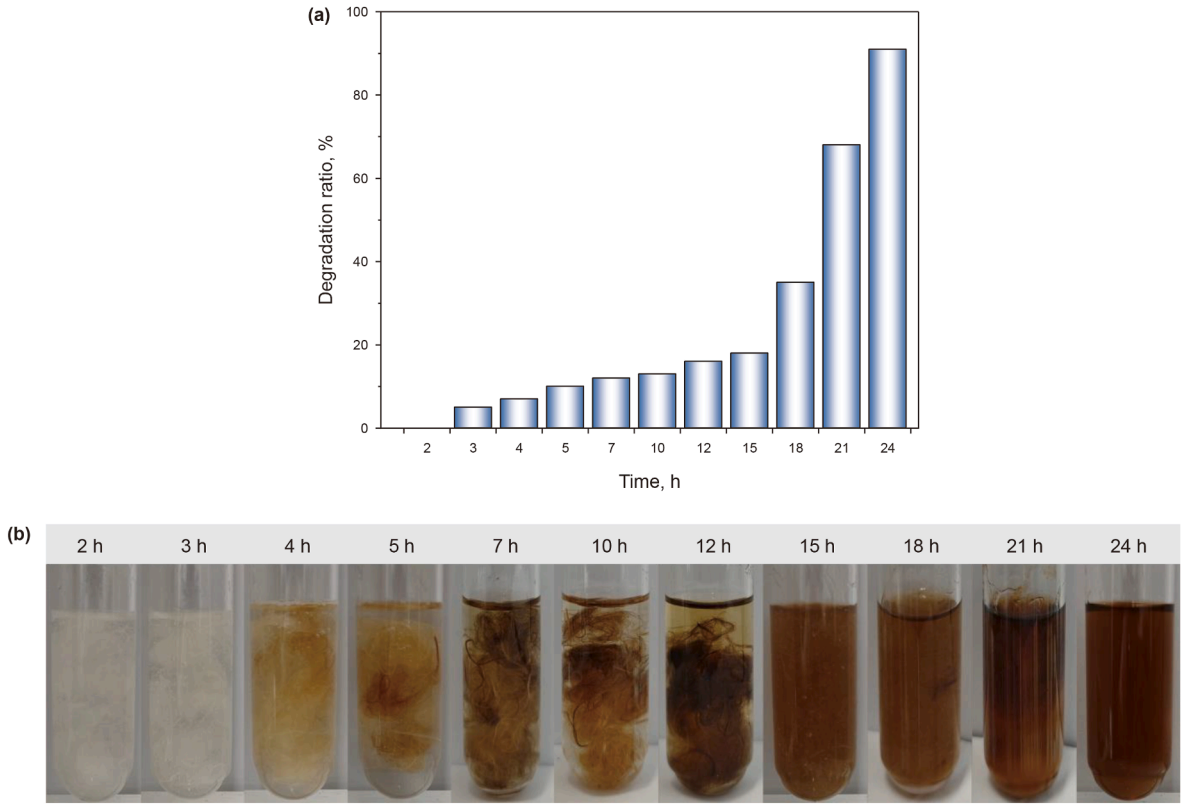

Fig. 13. Degradation ratio (**a**) and macroscopic states (**b**) of fibers aged in water at 180 °C for different durations.

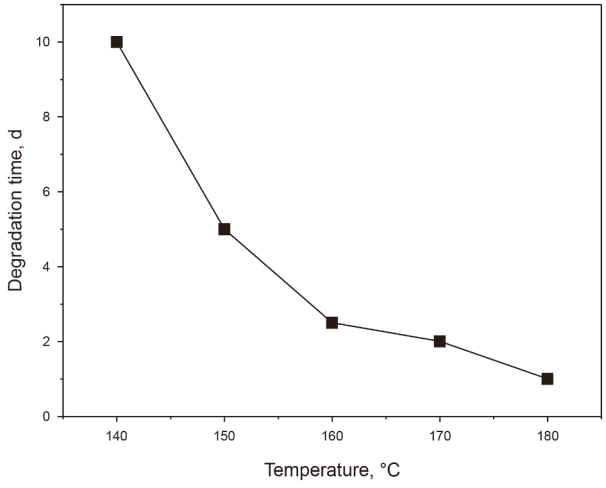

Fig. 14. Effect of temperature on the degradation time of fibers.

Fig. 15 illustrates the thermal degradation behavior of the composite plugging agent with a fiber concentration of 3 wt% at 180 °C. As shown in Fig. 15(a), the fibers in the system gradually degraded with increasing aging time. After 32 h, the system became transparent, indicating efficient fiber degradation. Fig. 15(b) shows the degradation behavior of the gel within the composite system. After efficient fiber degradation, the gel maintained a G-level strength for up to 72 h. After 100 h of aging, the gel network completely disintegrated, and the system ultimately degraded into a viscous liquid.

Fig. 16 compares the viscosity characteristics of the broken gel fluids after degradation of the composite plugging agent and the pure gel. Both fluids exhibit typical shear-thinning rheological behavior. At a shear rate of 7.6 s^{-1}, the viscosity of the degraded composite fluid was 49.2 mPa·s, slightly higher than that of the degraded pure gel fluid (43.9 mPa·s). This is mainly due to the presence of fiber degradation products. In addition, it can be observed from Fig. 16 that the viscosity exhibits an unexpected increase as the shear rate rises to 400 s^{-1}. This phenomenon can be attributed to the fact that polymer chains are fully stretched and oriented at high shear rates, which strengthens the intermolecular elastic effect and hydrodynamic interactions. Nevertheless, the viscosities of both fluids remain low, indicating favorable mobility within fractures after degradation and facilitating efficient flowback.

3.4. Strength enhancement mechanism of gel–fiber composite system

Fig. 17 presents the microscopic morphology of the composite temporary plugging agent. The images reveal that the gel matrix uniformly fills the inter-fiber spaces and intertwines with the fibers to form a dense three-dimensional network. This structure significantly reduces the internal pore size of the composite

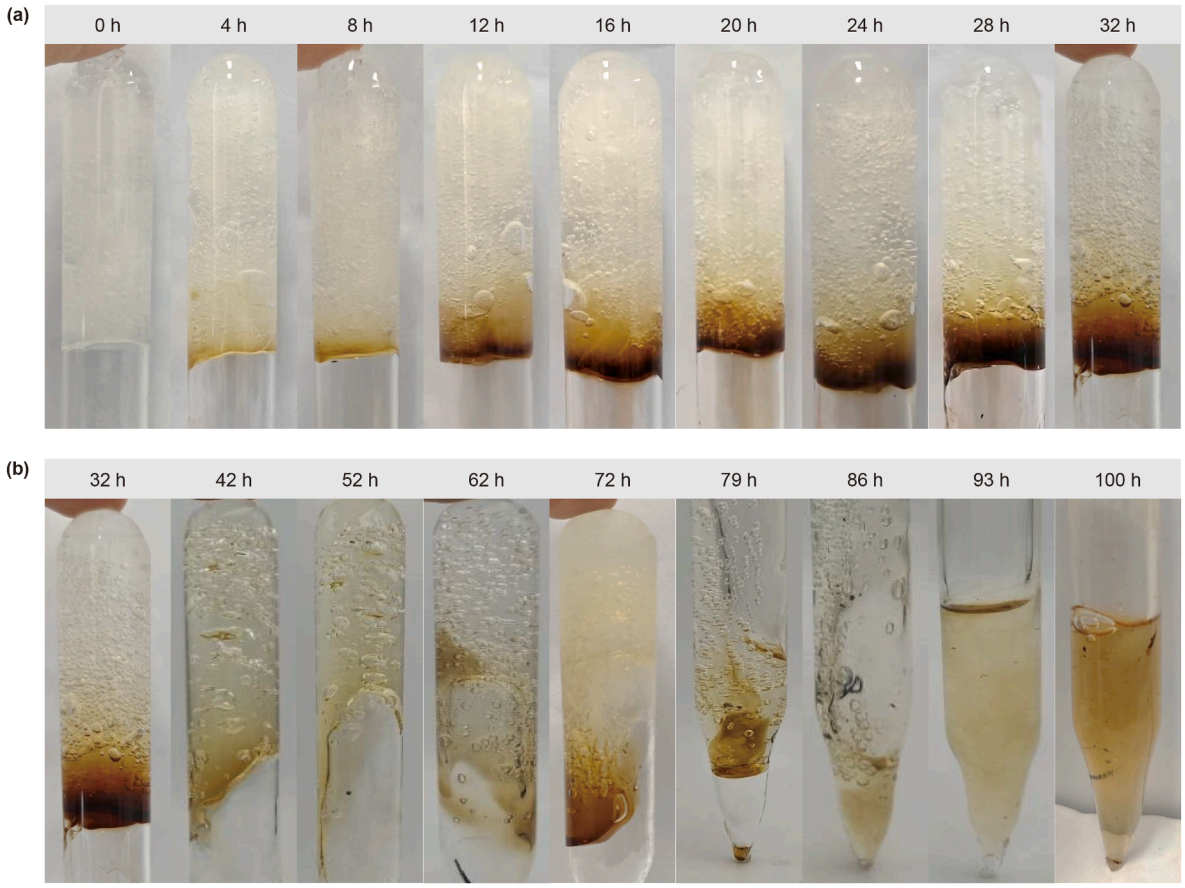

Fig. 15. Degradation process of fibers (**a**) and gel (**b**) within the composite system at 180 °C.

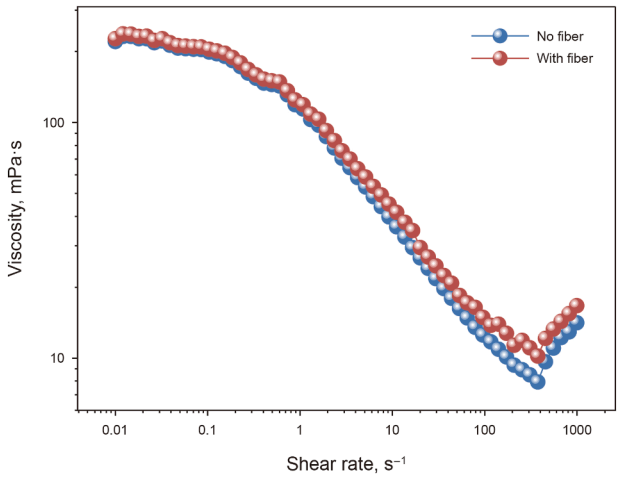

Fig. 16. Shear-dependent rheological viscosity of fluids after efficient degradation of the composite temporary plugging agent and the pure gel.

system. Simultaneously, the gel forms an interfacial adhesive layer on the fiber surfaces, effectively bridging adjacent fibers and enhancing the structural integrity and mechanical strength of the composite. The filling effect of the gel reduces the porosity of the filter cake, while the interfacial adhesion strengthens the bonding between fibers. Together, these mechanisms provide robust structural support, enabling the composite plugging agent to withstand external pressure and maintain a stable sealing layer during the plugging process.

Fig. 18 presents the diameter distribution of the fibers before and after gel formation. The experimental results show that prior to gelation, the fiber diameters were primarily distributed in the range of 9–12 μm. After gelation, the fiber diameters mainly fell within the range of 25–28 μm, indicating a clear increase in apparent diameter. During the gelation process, the gel matrix coats the fiber surfaces, forming a coating layer. This coating not only directly increases the apparent fiber diameter but also strengthens the physical entanglement and interactions between fibers through interfacial adhesion. This enhancement provides critical structural support, thereby contributing to the improved mechanical strength and stability of the composite temporary plugging agent.

Fig. 19 presents the infrared spectra of the composite temporary plugging agent, pure fibers, and pure gel. The infrared spectrum of the composite is essentially identical to that of the pure gel. Distinct absorption peaks appear at 3335 and 3194 cm^{-1}, which correspond to the stretching vibrations of N–H in amide groups. A peak at 2927 cm^{-1} is attributed to the stretching vibration of saturated C–H bonds. The peak at

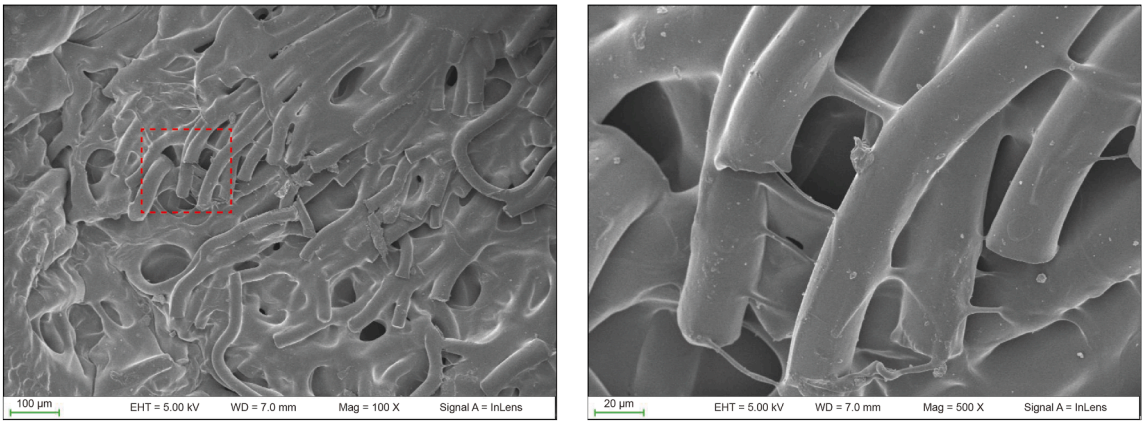

Fig. 17. Microstructural features of the gel–fiber interwoven network in the composite system.

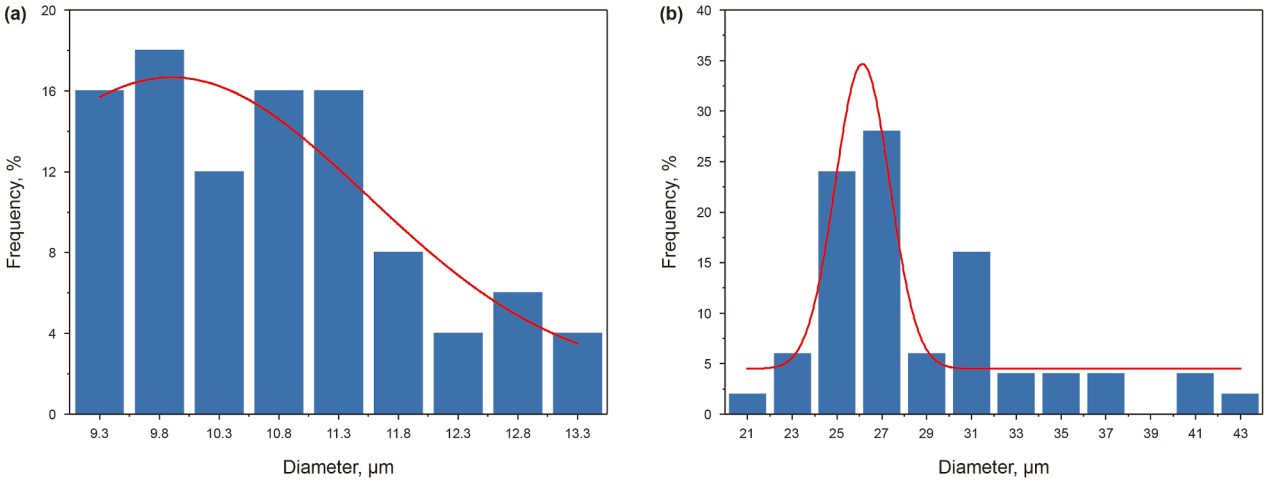

Fig. 18. Diameter distribution of fibers before (**a**) and after (**b**) gelation in the composite system.

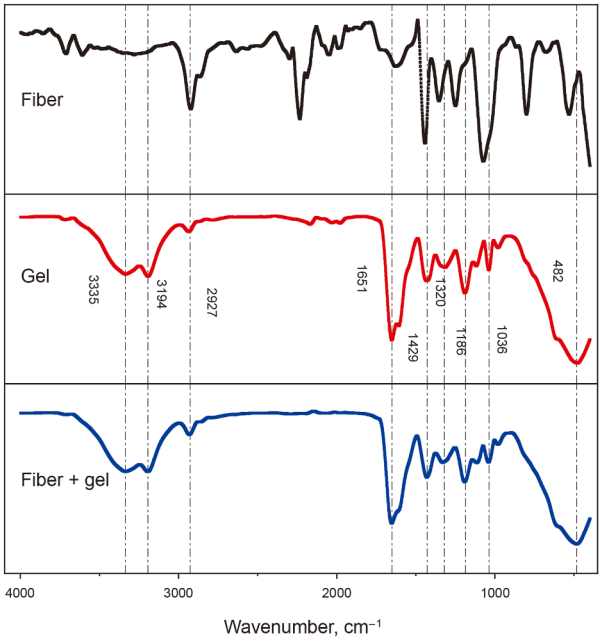

Fig. 19. Comparison of infrared spectra among the composite system, pure gel, and pure fibers.

1651 cm^{-1} is attributed to the C=O stretching vibration, while the peaks at 1036 and 1186 cm^{-1} are characteristic of $-SO_3Na$ groups.

Fig. 20 summarizes the synergistic plugging and reinforcement mechanisms of the gel–fiber composite system at both the fracture inlet and within the fracture interior. As illustrated in Fig. 20(a), the composite system is capable of forming effective plugs at both locations. For narrow fractures, geometric restriction at the fracture inlet promotes rapid interception and accumulation of fibers, leading to the formation of a composite plug at the entrance. In contrast, for wider fractures, fibers are able to penetrate into the fracture interior, where they are progressively captured through friction with the fracture walls and inter-fiber entanglement, ultimately forming a composite plug within the fracture.

As further illustrated in Fig. 20(b), the gel substantially reinforces the mechanical strength of the fiber bridging structure. The gel constrains the movement of the fiber bridging structure, while the fiber bridging structure in turn dissipates impact forces acting on the gel. Such synergistic interaction gives rise to significantly improved plugging strength and shear strength of the composite system. This synergy eliminates the strict particle-size matching requirement and enables robust and adaptable sealing under complex fracture conditions.

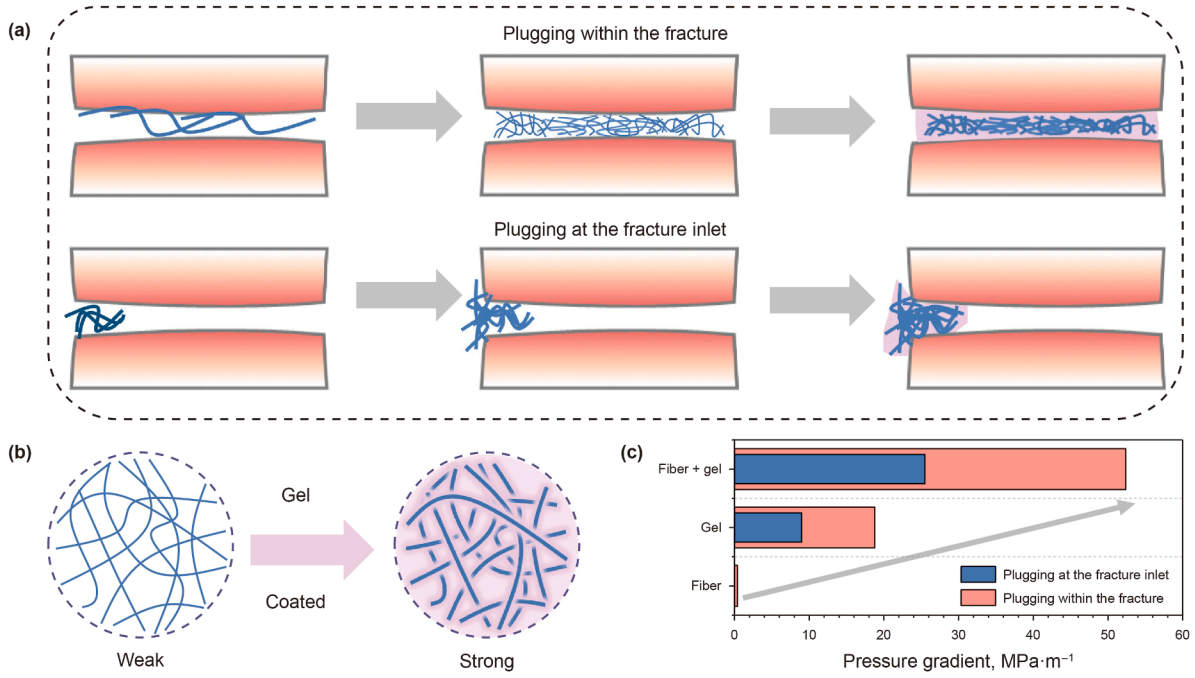

Fig. 20. (**a**) Schematic of the fiber capture process within fractures; (**b**) the reinforcement mechanism of the composite system; (**c**) comparison of plugging capabilities of different systems (8 wt% monomer concentration, 3 wt% fiber concentration, 2 mm fracture width).

4. Conclusions

To address the challenge of balancing plugging strength and fracture adaptability in existing temporary plugging agents, this study developed a high-temperature degradable gel–fiber composite system based on in situ polymerization. By dispersing fibers in a low-viscosity gelling fluid, the system can be effectively injected into the internal region of the fracture. Upon exposure to reservoir temperature, the system rapidly polymerizes to form a fiber-reinforced three-dimensional gel network. The main findings of this study are summarized as follows.

(1) The optimized gelling fluid maintains low viscosity during preparation and pumping. At 180 °C, it rapidly gels within 0.33 h, demonstrating good injectability and controllable gelation behavior.
(2) Through physical entanglement and interfacial bonding, fibers significantly enhance the mechanical properties of the gel matrix. When the fiber concentration reaches 3 wt% or higher, the elastic modulus of the composite increases by one order of magnitude, and the system exhibits excellent cyclic shear stability.
(3) Fracture plugging tests show that fiber incorporation increases plugging strength by 2.8–3.4 times compared with the pure gel system. In fractures with widths of 2–3 mm, the plugging pressure gradient exceeds 49 MPa·m^{-1}, effectively extending the applicable fracture width range of the plugging agent.
(4) All components in the system exhibit good thermal degradability. At 180 °C, the composite fully degrades into a low-viscosity liquid within 100 h, facilitating the restoration of fracture conductivity.

CRediT authorship contribution statement

Yu-Hui Yang: Writing – review & editing, Writing – original draft, Visualization, Project administration, Methodology, Investigation, Formal analysis, Data curation, Conceptualization. **Jun-Cheng Su:** Visualization, Investigation, Formal analysis, Data curation. **Shan-Sheng Xu:** Writing – original draft, Investigation, Formal analysis, Data curation. **Zhi-Yi Wei:** Methodology, Investigation, Formal analysis, Data curation. **Chu-Yu Kang:** Visualization, Investigation, Data curation. **Zhuo-Zhuang Liu:** Visualization, Investigation, Conceptualization. **Jie Geng:** Visualization, Resources, Project administration, Formal analysis, Conceptualization. **Hai Huang:** Visualization, Resources, Project administration, Formal analysis. **Hai-Ming Fan:** Visualization, Methodology, Investigation, Funding acquisition, Formal analysis, Conceptualization.

Data availability

Data will be made available on request.

Declaration of competing interest

No conflict of interest exists in the submission of this manuscript, and the manuscript is approved by all authors for publication. I would like to declare on behalf of my co-authors that the work described was original research that has not been published previously, and is not under consideration for publication elsewhere, in whole or in part. All the authors listed have approved the manuscript that is enclosed.

Acknowledgments

This work was supported by the Key Project of National Natural Science Foundation of China (No. 52434002) and the National Key Research and Development Program of China (2019YFA0708700).

References

Chen, L., Huang, F., Li, G., et al., 2023. Experimental study on fiber balls for bridging in fractured-vuggy reservoir. SPE J. 28 (4), 1880–1894. https://doi.org/10.2118/214315-PA.

Chen, X., Lu, X., Liu, P.L., et al., 2024. A critical review of key points in temporary plugging fracturing: Materials, injection, temporary plugging, and design. Geoenergy Sci. Eng. 240, 212981. https://doi.org/10.1016/j.geoen.2024.212981.

Cohen, C.E., Tardy, P.M., Lesko, T., et al., 2010. Understanding diversion with a novel fiber-laden acid system for matrix acidizing of carbonate formations. In: SPE Annual Technical Conference and Exhibition. https://doi.org/10.2118/134495-MS.

Feng, W., Yang, C., Zhou, F., 2021. Experimental study on surface morphology and relevant plugging behavior within acid-etched and unetched fractures. J. Nat. Gas Sci. Eng. 88, 103847. https://doi.org/10.1016/j.jngse.2021.103847.

Gussenov, I.S., Seright, R.S., 2024. Permeability reduction techniques: Plain and fiber HPAM gels in fractured cores. Geoenergy Sci. Eng. 234, 212565. https://doi.org/10.1016/j.geoen.2023.212565.

Huo, J., Zhang, H., Wei, C., et al., 2025. Oil-soluble temporary plugging agent used for drilling reservoir protection: Preparation, characteristics and mechanism. J. Appl. Polym. Sci. 142 (42), e57611. https://doi.org/10.1002/app.57611.

Kibikas, W., Ingraham, M., 2025. Compaction and morphology of lost circulation materials. SPE J. 30 (10), 6014–6027. https://doi.org/10.2118/228435-PA.

Li, J., Yang, H., Qiao, Y., et al., 2018. Laboratory evaluations of fiber-based treatment for in-depth profile control. J. Pet. Sci. Eng. 171, 271–288. https://doi.org/10.1016/j.petrol.2018.07.060.

Li, J.B., Luo, Z.F., Fu, H.R., et al., 2024. Research and application of the low-damage temperature-controlled phase change temporary plugging agent. Geoenergy Sci. Eng. 241, 213122. https://doi.org/10.1016/j.geoen.2024.213122.

Li, M., Zhou, F.-J., Sun, Z., et al., 2022. Experimental study on plugging performance and diverted fracture geometry during different temporary plugging and diverting fracturing in Jimusar shale. J. Pet. Sci. Eng. 215, 110580. https://doi.org/10.1016/j.petrol.2022.110580.

Li, M., Guo, J., Zhou, F., et al., 2023. Experimental study on plugging behavior of degradable diverters in partially open fracture in temporary plugging and diverting fracturing. ACS Omega 8 (15), 14066–14076. https://doi.org/10.1021/acsomega.3c00689.

Li, W., Liu, Y., Meng, Q., et al., 2025. Study on migration and plugging mechanism of knot temporary plugging agent in hydraulic fracturing. Phys. Fluids 37 (6), 063349. https://doi.org/10.1063/5.0270811.

Peng, Y., Ye, J., Li, Y., et al., 2025. Development and performance evaluation of novel self-degradable preformed particulate gels with high-temperature and high-salinity resistance. SPE J. 30 (3), 1105–1115. https://doi.org/10.2118/224404-PA.

Ren, L., Peng, S., Zhao, J., et al., 2024. Optimization design of plugging agent dosage and application of deep shale gas inner-diversion fracturing. Geoenergy Sci. Eng. 239, 212908. https://doi.org/10.1016/j.geoen.2024.212908.

Sydansk, R.D., 1988. A new conformance-improvement-treatment chromium (III) gel technology. In: SPE Enhanced Oil Recovery Symposium. https://doi.org/10.2118/17329-MS.

Tian, A., Fu, G., Tang, J., et al., 2024. Numerical simulation of the transport and sealing law of temporary plugging particles in complex fractures of carbonate-type thermal storage. Energies 17 (13), 3283. https://doi.org/10.3390/en17133283.

Wang, B., Zhang, G., Sun, Z., et al., 2023a. Plugging characteristics of self-degradable diverters within three-dimensional hydro-fractures: An experimental investigation. Phys. Fluids 35 (9), 093311. https://doi.org/10.1063/5.0168463.

Wang, D.-B., Qin, H., Wang, Y.-L., et al., 2023b. Experimental study of the temporary plugging capability of diverters to block hydraulic fractures in high-temperature geothermal reservoirs. Pet. Sci. 20 (6), 3687–3699. https://doi.org/10.1016/j.petsci.2023.07.002.

Wang, G., He, S., Yu, J., et al., 2024a. *In-situ* poly(hexahydrotriazine) gels temporary plugging agent suitable for high-temperature reservoirs: Regulation by inorganic chloride salts. Geoenergy Sci. Eng. 239, 212905. https://doi.org/10.1016/j.geoen.2024.212905.

Wang, Y., Fan, Y., Wang, X., 2023c. Study on migration law of multiscale temporary plugging agent in rough fractures of shale oil reservoirs. Front. Phys. 11, 1228006. https://doi.org/10.3389/fphy.2023.1228006.

Wang, Y., Song, H., Zhou, F., 2024b. Geometric characteristics of diverting fractures for multi-stage dynamic temporary plugging and diverting fracturing in fractured reservoir. Phys. Fluids 36 (3), 037107. https://doi.org/10.1063/5.0195980.

Wang, Y., Yuan, Q., Chen, W., et al., 2025. Temporary-plugging-driven balanced fracturing: A novel strategy to achieve uniform reservoir stimulation in Sichuan Shale oil horizontal wells. Processes 13 (6), 1846. https://doi.org/10.3390/pr13061846.

Xu, H., Jiang, H., Wang, J., et al., 2023. Formulation optimization of materials used in temporary plugging diversion between fracture front end and cluster in shale gas: From laboratory research to field application. Phys. Fluids 35, 063310. https://doi.org/10.1063/5.0151878.

Xu, W., Jiang, F., Wang, L., et al., 2024. Experimental study on plugging behavior of multitype temporary plugging agents in hydraulic fractures. SPE J. 29 (12), 6756–6774. https://doi.org/10.2118/223625-PA.

Yang, C., Zhou, F., Feng, W., et al., 2019. Plugging mechanism of fibers and particulates in hydraulic fracture. J. Pet. Sci. Eng. 176, 396–402. https://doi.org/10.1016/j.petrol.2019.01.084.

Yang, C., Feng, W., Zhou, F.J., 2020. Formation of temporary plugging in acid-etched fracture with degradable diverters. J. Pet. Sci. Eng. 194, 107535. https://doi.org/10.1016/j.petrol.2020.107535.

Yang, Y., Fan, H., Su, J., et al., 2026. High-strength and controllable thermal degrading hydrogel for temporary plugging in ultra-high-temperature reservoirs. Colloids Surf. A Physicochem. Eng. Aspects 728, 138493. https://doi.org/10.1016/j.colsurfa.2025.138493.

Zhang, H.-J., Zhu, D.-Y., Gong, Y.-L., et al., 2022a. Degradable preformed particle gel as temporary plugging agent for low-temperature unconventional petroleum reservoirs: Effect of molecular weight of the cross-linking agent. Pet. Sci. 19 (6), 3182–3193. https://doi.org/10.1016/j.petsci.2022.07.013.

Zhang, L., Zhou, F., Feng, W., et al., 2020. Experimental study on plugging behavior of degradable fibers and particulates within acid-etched fracture. J. Pet. Sci. Eng. 185, 106455. https://doi.org/10.1016/j.petrol.2019.106455.

Zhang, X., Deng, J.-N., Yang, K., et al., 2022b. High-strength and self-degradable sodium alginate/polyacrylamide preformed particle gels for conformance control to enhance oil recovery. Pet. Sci. 19 (6), 3149–3158. https://doi.org/10.1016/j.petsci.2022.06.012.

Zhao, F., Chen, W., Zeng, J., et al., 2025a. Study on the influence mechanism of fiber properties on the strength of fiber-particle composite temporary plugging layer. In: ADIPEC. https://doi.org/10.2118/229707-MS.

Zhao, J., Huang, Y., Ren, L., et al., 2025b. Behavior analysis of fine temporary plugging agents and fibers in bridging regions: Migration and clogging. In: ADIPEC. https://doi.org/10.2118/229552-MS.

Zhao, S., Al Brahim, A., Liu, J., et al., 2023. Coreflooding evaluation of fiber-assisted recrosslinkable preformed particle gel using an open fracture model. SPE J. 28 (1), 268–278. https://doi.org/10.2118/212282-PA.

Zhou, H., Wu, X., Song, Z., et al., 2022. A review on mechanism and adaptive materials of temporary plugging agent for chemical diverting fracturing. J. Pet. Sci. Eng. 212, 110256. https://doi.org/10.1016/j.petrol.2022.110256.

Zhou, Q., Luo, Z., Fu, H., et al., 2025. Research and application progress of temporary plugging agent for acidification fracturing: A review. Geoenergy Sci. Eng. 247, 213600. https://doi.org/10.1016/j.geoen.2024.213600.

Zou, Y., Li, Y., Yang, C., et al., 2024a. Fracture propagation law of temporary plugging and diversion fracturing in shale reservoirs under completion experiments of horizontal well with multi-cluster sand jetting perforation. Petrol. Explor. Dev. 51 (3), 715–726. https://doi.org/10.1016/S1876-3804(24)60500-8.

Zou, Y., Zhao, Z., Zhang, S., et al., 2024b. Adjustment of fracture network geometry during temporary plugging and diverting fracturing in deep coalbed methane reservoirs: An experimental study. Phys. Fluids 36, 126628. https://doi.org/10.1063/5.0244637.

Zou, Y.-S., Yang, C., Zhang, S.-C., et al., 2024c. Multi-fracture growth behavior during TPDF in a horizontal well of multi-clustered perforations: An experimental research. Pet. Sci. 21 (6), 4230–4247. https://doi.org/10.1016/j.petsci.2024.08.003.